

# $^{124}\text{I}$ -Labeled Engineered Anti-CEA Minibodies and Diabodies Allow High-Contrast, Antigen-Specific Small-Animal PET Imaging of Xenografts in Athymic Mice

Gobalakrishnan Sundaresan, PhD<sup>1</sup>; Paul J. Yazaki, PhD<sup>2</sup>; John E. Shively, PhD<sup>2,3</sup>; Ronald D. Finn, PhD<sup>4</sup>; Steven M. Larson, MD<sup>4</sup>; Andrew A. Raubitschek, MD<sup>2,3</sup>; Lawrence E. Williams, PhD<sup>2</sup>; Arion F. Chatziioannou, PhD<sup>1</sup>; Sanjiv S. Gambhir, MD, PhD<sup>1,5,6</sup>; and Anna M. Wu, PhD<sup>1-3,5</sup>

<sup>1</sup>Crump Institute for Molecular Imaging, Department of Molecular and Medical Pharmacology, David Geffen School of Medicine at UCLA, Los Angeles, California; <sup>2</sup>Beckman Research Institute, City of Hope National Medical Center, Duarte, California; <sup>3</sup>City of Hope Comprehensive Cancer Center, Duarte, California; <sup>4</sup>Radiopharmaceutical Chemistry Service and Nuclear Medicine Service, Department of Radiology, Memorial Sloan-Kettering Cancer Center, New York, New York; <sup>5</sup>UCLA Jonsson Comprehensive Cancer Center, David Geffen School of Medicine at UCLA, Los Angeles, California; and <sup>6</sup>Department of Radiology and Bio-X Program, Stanford University, Stanford, California

Prolonged clearance kinetics have hampered the development of intact antibodies as imaging agents, despite their ability to effectively deliver radionuclides to tumor targets in vivo. Genetically engineered antibody fragments display rapid, high-level tumor uptake coupled with rapid clearance from the circulation in the athymic mouse/LS174T xenograft model. The anticarcinoembryonic antigen (CEA) T84.66 minibody (single-chain Fv fragment [scFv]-C<sub>H</sub>3 dimer, 80 kDa) and T84.66 diabody (non-covalent dimer of scFv, 55 kDa) exhibit pharmacokinetics favorable for radioimmunoimaging. The present work evaluated the minibody or diabody labeled with  $^{124}\text{I}$ , for imaging tumor-bearing mice using a high-resolution small-animal PET system. **Methods:** Labeling was conducted with 0.2–0.3 mg of protein and 65–98 MBq (1.7–2.6 mCi) of  $^{124}\text{I}$  using an iodination reagent. Radiolabeling efficiencies ranged from 33% to 88%, and immunoreactivity was 42% (diabody) or >90% (minibody). In vivo distribution was evaluated in athymic mice bearing paired LS174T human colon carcinoma (CEA-positive) and C6 rat glioma (CEA-negative) xenografts. Mice were injected via the tail vein with 1.9–3.1 MBq (53–85  $\mu\text{Ci}$ ) of  $^{124}\text{I}$ -minibody or with 3.1 MBq (85  $\mu\text{Ci}$ ) of  $^{124}\text{I}$ -diabody and imaged at 4 and 18 h by PET. Some mice were also imaged using  $^{18}\text{F}$ -FDG 2 d before imaging with  $^{124}\text{I}$ -minibody. **Results:** PET images using  $^{124}\text{I}$ -labeled minibody or diabody showed specific localization to the CEA-positive xenografts and relatively low activity elsewhere in the mice, particularly by 18 h. Target-to-background ratios for the LS174T tumors versus soft tissues using  $^{124}\text{I}$ -minibody were 3.05 at 4 h and 11.03 at 18 h. Similar values were obtained for the  $^{124}\text{I}$ -diabody (3.95 at 4 h and 10.93 at 18 h). These results were

confirmed by direct counting of tissues after the final imaging. Marked reduction of normal tissue activity, especially in the abdominal region, resulted in high-contrast images at 18 h for the  $^{124}\text{I}$ -anti-CEA diabody. CEA-positive tumors as small as 11 mg (<3 mm in diameter) could be imaged, and  $^{124}\text{I}$ -anti-CEA minibodies, compared with  $^{18}\text{F}$ -FDG, demonstrated highly specific localization. **Conclusion:**  $^{124}\text{I}$  labeling of engineered antibody fragments provides a promising new class of tumor-specific probes for PET imaging of tumors and metastases.

**Key Words:** radioimmunoimaging; engineered antibody fragments; carcinoembryonic antigen;  $^{124}\text{I}$ ; PET

J Nucl Med 2003; 44:1962–1969

**R**adioimmunopharmaceuticals represent a promising class of agents for cancer diagnosis, offering the possibility of discrimination between normal and malignant tissues based on specific antigen expression. Recombinant approaches can be used to modify many characteristics of monoclonal antibodies to optimize them for in vivo targeting (1,2). In particular, engineered fragments can be produced that demonstrate rapid uptake into tumors and fast clearance from blood and nontarget tissues, key characteristics required of an imaging agent (2).

Single-chain Fv fragments (scFv), consisting of the variable regions of the immunoglobulin light and heavy chains tethered via a short peptide linker, have been derived from an array of antitumor antibodies and evaluated for in vivo targeting in tumor xenograft-bearing mice (3). Because scFvs are smaller (25–30 kDa) than intact IgG (150 kDa), they show improved tissue penetration (4) and rapid clearance from circulation, resulting in improved tumor-to-blood ratios. However, because

Received Feb. 26, 2003; revision accepted Jun. 13, 2003.

For correspondence or reprints contact: Anna M. Wu, PhD, Crump Institute for Molecular Imaging, David Geffen School of Medicine at UCLA, 700 Westwood Plaza, Crump A342B, P.O. Box 951770, Los Angeles, CA 90095-1770. E-mail: awu@mednet.ucla.edu

of their monovalent nature and rapid elimination from the circulation, scFvs demonstrate substantially lower tumor uptakes than does the corresponding intact IgG (3).

Antitumor diabodies (noncovalent dimers of scFv fragments, 55 kDa), formed by using short linker peptides to promote cross-pairing, show tumor uptakes superior to those of their scFv counterparts and retain rapid blood clearance (2). This leads to high tumor-to-blood ratios at early times after administration. Larger fragments such as the minibody (scFv-CH3; 80 kDa) (5) and scFv-Fc (110 kDa) (6) fusion proteins can demonstrate even higher tumor uptakes; localization is improved because of the longer serum half-lives of these species, allowing longer exposure of the target tissue to the antibody fragment. The trade-off, however, is that longer intervals are required between administration and image acquisition for optimal contrast.

PET is well established as an imaging modality, offering high sensitivity and resolution; furthermore, tissue uptakes can be quantitated using PET.  $^{18}\text{F}$  (half-life, 109 min) has been the favored radionuclide for labeling of small molecule tracers. However, the slower targeting and clearance kinetics of biomolecules, including antibodies and fragments, has prompted the evaluation of intermediate-half-life positron emitters including  $^{64}\text{Cu}$  (half-life, 12.7 h) and  $^{124}\text{I}$  (half-life, 4.18 d) for PET imaging. In particular, targeting and imaging of  $^{124}\text{I}$ -labeled intact antibodies have been evaluated preclinically in animal models of breast or ovarian cancer (7–9) and in humans (10) using clinical PET scanners. However, PET imaging applications using  $^{124}\text{I}$  may be hampered by the relatively low positron yield (23%), low inherent resolution due to high energy and longer range of the positron emission, and quantitation issues arising from  $\gamma$ -rays emitted in coincidence with positrons or with other  $\gamma$ -emissions (11). The high  $\gamma$ -emissions also raise issues of high radiation doses and additional shielding requirements. Furthermore, the availability of  $^{124}\text{I}$  is currently limited to research purposes only. Nonetheless, development of trac-

ers labeled with positron emitters of longer half-life remains an important goal in PET.

In our previous work, diabodies and minibodies were generated from the anticarcinoembryonic antibody (CEA) T84.66. These were radiolabeled with  $^{123}\text{I}/^{131}\text{I}$  or conjugated with 1,4,7,10-tetraazacyclododecane *N,N',N'',N'''*-tetraacetic acid (DOTA) for radiolabeling with  $^{111}\text{In}$ . The T84.66 diabody (55 kDa) showed rapid tumor localization in athymic mice bearing CEA-positive LS174T human colon carcinoma xenografts, reaching  $13.68 \pm 1.49$  percentage injected dose per gram of tissue (%ID/g) ( $^{123}\text{I}$ ) or  $12.5 \pm 0.4$  %ID/g ( $^{111}\text{In}$ ) 2 h after administration (5,12,13). The larger T84.66/GS18 Flex minibody (80 kDa; above the threshold for renal filtration) reached tumor accumulations of  $26.23 \pm 4.57$  %ID/g ( $^{131}\text{I}$ ) or  $24.47 \pm 6.1$  %ID/g ( $^{111}\text{In}$ ) at 12 h after injection (13). However, in radiometal-labeled forms, these fragments exhibited normal tissue retention as seen for other radiometal-labeled antibody fragments (1,14). In particular, the  $^{111}\text{In}$ -minibody showed elevated retention of activity in the liver ( $25.97 \pm 0.99$  %ID/g at 24 h), and the  $^{111}\text{In}$ -diabody reached very high levels of activity in the kidney ( $>180$  %ID/g at 6 h) (13). PET imaging studies confirmed the hepatic accumulation of  $^{64}\text{Cu}$ -DOTA-T84.66 (15). Because neither renal nor hepatic accumulation was significant for radioiodine-conjugated fragments, evaluation using a positron-emitting isotope of iodine was warranted. The combination of  $^{124}\text{I}$ -labeled anti-CEA diabody or anti-CEA minibody and PET imaging should take advantage of the favorable biologic properties of these radioiodinated proteins, including rapid reduction of activity in nonspecific tissues and organs.

## MATERIALS AND METHODS

### Production and Purification of T84.66 Minibody and Diabody

The anti-CEA scFv-CH3 minibody and diabody (shown schematically in Fig. 1) used in these studies were produced and

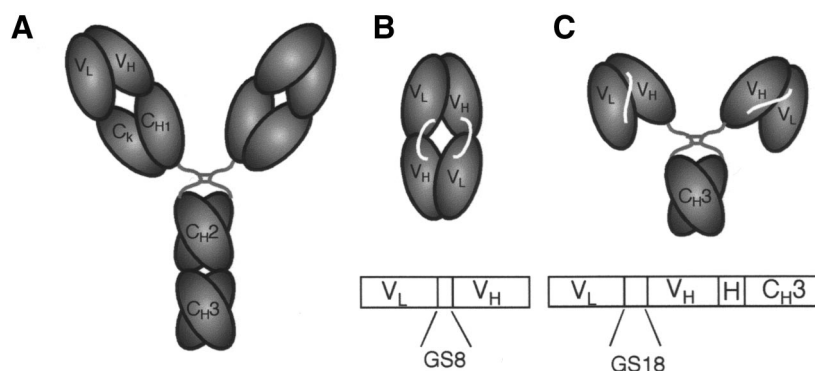


**FIGURE 1.** Schematic drawing shows domain structure of parental intact T84.66 antibody (A), T84.66 diabody (B), and T84.66 minibody (C). Anti-CEA minibody (80 kDa) and diabody (55 kDa) were derived from T84.66, a high-affinity and highly specific antibody that recognizes an epitope on A3 domain of CEA. Minibody (C) has glycine-serine-rich 18-amino-acid linker (GS18) between variable light ( $V_L$ ) and variable heavy chains ( $V_H$ ) and human IgG1 hinge (H) joining them to CH3 domain, also derived from human IgG1. Gene encoding diabody (B) encodes glycine-serine-rich 8-amino-acid linker (GS8) between  $V_L$  and  $V_H$  regions. Amino acid sequence is GSTSGGGSGGGSGGGSS for GS18 and GGGSGGGG for GS8.

purified as previously described in detail (16). Briefly, the T84.66/GS18 minibody and diabody were expressed in NS0 murine myeloma cells using the pEE12 expression vector and a cytomegalovirus promoter and glutamine synthetase as the selectable marker (Lonza Biologics) (17). Protein was purified by hydrophobic interaction chromatography (Source ISO; Amersham Pharmacia Biotech) followed by anion exchange chromatography (HQ50; PE Biosystems) using a BioCAD 700E perfusion chromatography system (PE Biosystems). Activity was determined by enzyme-linked immunosorbent assay using microtiter wells coated with a recombinant CEA protein (N and A3 domains) (18) and antihuman Fc (minibody) or antimurine Fab (diabody) (Jackson ImmunoResearch) for detection.

### Radioiodination of T84.66 Minibody and Diabody

Radioiodination of the engineered antibody fragments was accomplished by the IODO-GEN method (Pierce Biotechnology) as previously described (12). Carrier-free  $^{124}\text{I}$  was produced at the Cyclotron Facility of Memorial Sloan-Kettering Cancer Center as previously described (19). Labeling reactions (0.1–0.2 mL) typically contained 0.2–0.3 mg of purified protein and 65–98 MBq (1.75–2.65 mCi) of  $^{124}\text{I}$ . Radioiodinated proteins were purified by size-exclusion high-performance liquid chromatography (HPLC) on either a TSK2000 (Tosoh Biosep) or Superdex 75 (Amersham Biosciences) column, with phosphate-buffered saline (PBS)/1% human serum albumin (HSA) as the running buffer. The radiolabeling efficiency was determined by integrating areas on the HPLC trace and determining the radioactivity associated with the 80-kDa protein peak for minibody or 55-kDa peak for diabody as a percentage of total radioactivity eluted. Immunoreactivity was determined by incubation of the labeled protein with a 20-fold excess (w/w) of either purified CEA or the recombinant N-A3 fragment of CEA in 0.15 mL of PBS/1% HSA as previously described. Samples were analyzed by size-exclusion HPLC on tandem Superose 6 HR 10/30 columns (Amersham Biosciences) to assess formation of Ab:Ag complexes.

### Cell Lines and Xenografts

The LS174T human colorectal carcinoma cell line (CL 188) and C6 rat glioma cell line (CCL 107) were obtained from the American Type Culture Collection and maintained under standard conditions. Xenografts were established in 8-wk-old CD1 female nude mice (Charles River Laboratories) by subcutaneous inoculation of  $1\text{--}2 \times 10^6$  cells 10–14 d before the imaging studies. All animal handling and studies were performed in accordance with the guidelines of the University of California, Los Angeles (UCLA), Animal Research Committee.

### PET Scanning

Mice were imaged using the prototype small-animal PET scanner developed at the Crump Institute for Molecular Imaging, UCLA (20). Thyroid uptake of radioiodine was blocked by pretreatment using 10 drops of saturated KI per 100 mL of drinking water for 24 h before injection of radioiodinated protein. Stomach uptake was blocked by administration of 1.5 mg of potassium perchlorate in 0.2 mL of PBS by gastric lavage 30 min before injection. The mice were injected in the tail vein either with 1.9–3.1 MBq (53–85  $\mu\text{Ci}$ ) of  $^{124}\text{I}$ -minibody or with 3.1 MBq (85  $\mu\text{Ci}$ ) of  $^{124}\text{I}$ -diabody in saline/1% HSA. After the appropriate uptake time had elapsed, the mice were anesthetized by intraperitoneal injection of a mixture of ketamine (80 mg/kg final dose) and xylazine (10 mg/kg final dose), placed prone, and imaged using the

PET scanner with the long axis of the mouse parallel to the long axis of the scanner. Acquisition time was 28 min (4 min per bed position; 7 bed positions). Images were reconstructed using a 3-dimensional filtered backprojection reconstruction algorithm (21) for quantitation (see below) or using a *maximum a posteriori* reconstruction protocol (22) for presentation of images. Some mice were also imaged using  $^{18}\text{F}$ -FDG 2 d before the  $^{124}\text{I}$ -minibody scan. These were administered 5.6–7.4 MBq (150–200  $\mu\text{Ci}$ ) of  $^{18}\text{F}$ -FDG via the tail vein, and scans were acquired as described above, beginning 1 h after tracer injection. In some experiments, after scanning, the animals were euthanized; the tumors were excised, weighed, and counted in a well counter (Cobra II Auto-Gamma; Packard); and the %ID/g was calculated.

### Digital Whole-Body Autoradiography (DWBA)

The mice were sacrificed and frozen in carboxymethyl cellulose (Aldrich) in preparation for sectioning using a Cryostat (PMV). Coronal cross-sections were obtained with a thickness of 45  $\mu\text{m}$ . DWBA was performed using a Fujifilm BAS 5000 PhosphorImager (Fujifilm Medical Systems U.S.A., Inc.) and digital plates with a final resolution of  $\sim 100 \mu\text{m}$ . DWBA data were analyzed using Mac BAS software, version 2.4 (Fujifilm Medical Systems U.S.A., Inc.).

### Data Analysis

Preliminary quantitation of the small-animal PET images was performed using the Crump Institute Integrated Imaging Software Package, or CRIISP (Crump Institute for Molecular Imaging, UCLA). From the 3-dimensional filtered backprojection reconstruction, several planes (of a total of 64) encompassing the tumors were selected in the coronal orientation and averaged. Regions of interest (ROIs) were drawn for both the control and LS174T CEA-positive tumors centered on the peak of the activity profile. A soft-tissue region in the neck, as well as the area of maximum activity in the abdominal region, was also included for ROI analysis. Approximately equal-sized ROIs were drawn. ROI counts per pixel per minute were converted to counts per cubic centimeter per minute using a calibration factor obtained from scanning a cylinder containing a known amount of  $^{124}\text{I}$  activity. After decay correction, these data were converted to %ID/g by dividing by the known amount of injected activity. Target-to-background ratios were then determined for individual mice and averaged. The effects of ROI positioning were determined by averaging at least 3 ROIs and assessing the variability across regions. Statistical analysis was performed using the Excel 2000 (Microsoft) software package.

## RESULTS

### $^{124}\text{I}$ -Labeling of Anti-CEA Minibody and Diabody

As shown in Figure 2,  $^{124}\text{I}$  was readily conjugated to the T84.66 minibody and T84.66 diabody after short incubations (3–5 min). Specific activities after labeling ( $n = 3$ ) ranged from 81 to 133 kBq/ $\mu\text{g}$  (2.2–3.6  $\mu\text{Ci}/\mu\text{g}$ ). The immunoreactivity of the labeled protein, as determined by size-exclusion HPLC analysis after incubation with excess antigen, was >90% in the case of minibodies and 42% for diabodies.

### PET Imaging of Xenografts Using $^{124}\text{I}$ -Anti-CEA Minibody

To evaluate tumor targeting of the  $^{124}\text{I}$ -minibody, antigen-positive (LS174T colorectal carcinoma) and antigen-nega-

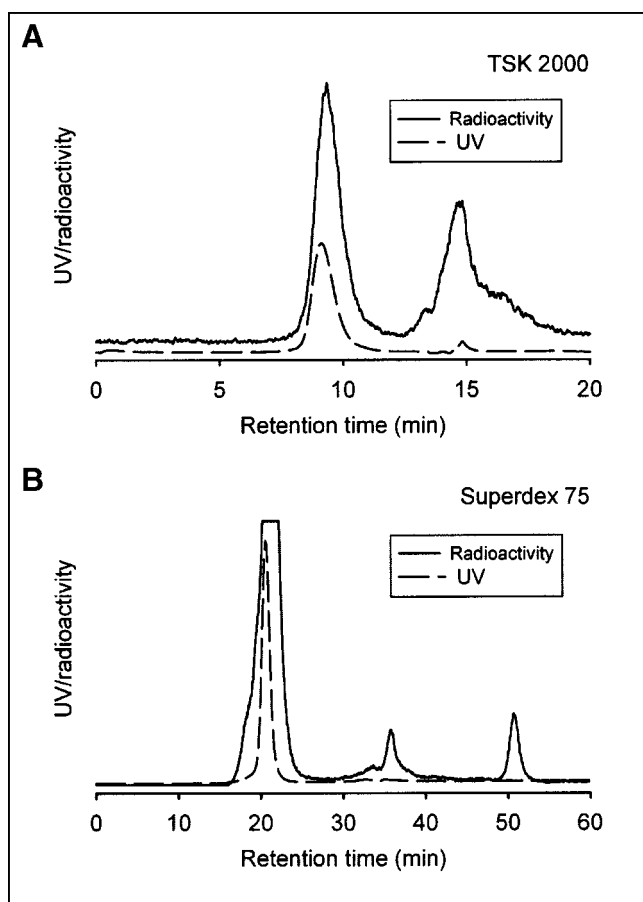


**FIGURE 2.** Size-exclusion HPLC analysis of  $^{124}\text{I}$ -radiolabeled anti-CEA minibody (A) and diabody (B).  $^{124}\text{I}$  was conjugated to T84.66 minibody and T84.66 diabody as described in Materials and Methods. Radiolabeling efficiency was determined by integrating areas on HPLC trace and determining radioactivity associated with 80-kDa protein peak for minibody or 55-kDa peak for diabody as percentage of total radioactivity eluted. Labeling efficiencies were 33% (not shown) or 46% for minibody (A) and 88% for diabody (B). Peak fractions (based on protein absorbance) were pooled for animal studies. Smaller peaks represent unincorporated label and low-molecular-weight components.

tive control (C6 glioma) xenografts were established by subcutaneous inoculation in athymic mice. PET imaging studies were conducted on animals bearing CEA-positive tumors averaging 142 mg (range, 11–487 mg). In one of the study phases, each of 4 mice was injected in the tail vein with  $\sim 2$  MBq (53  $\mu\text{Ci}$ ) of  $^{124}\text{I}$ -minibody, and whole-body PET scans were obtained beginning 4 and 18 h after administration. The image in Figure 3C clearly demonstrates high uptake into the positive (LS174T) tumor and low activity in the control (C6) tumor. The positive tumor-to-control tumor uptake ratio for the  $^{124}\text{I}$ -anti-CEA minibody was 3.46:1 at 4 h and 10.85:1 at 18 h, demonstrating high specificity ( $n = 8$ ; Table 1).

Comparison of the PET image encompassing the C6 and LS174T xenografts, and a corresponding DWBA section (Fig. 3E), clearly demonstrates that the region of high uptake observed in the scan correlates with autoradiographically detected tumor-associated radioactivity. Furthermore, an  $^{18}\text{F}$ -FDG PET scan of the same animal, performed before the  $^{124}\text{I}$ -minibody scan, allowed visualization of both tumors (Fig. 3B). The accumulation of  $^{18}\text{F}$ -FDG activity in the control and CEA-positive tumors was not significantly different. These studies confirm that the observed high localization of the  $^{124}\text{I}$ -minibody was antigen specific.

#### Visualization of CEA-Positive Xenografts Using $^{124}\text{I}$ -Anti-CEA Diabody

Experiments were conducted similarly using the  $^{124}\text{I}$ -anti-CEA diabody in animals ( $n = 4$ ) bearing CEA-positive tumors with an average weight of 183 mg (range, 40–420 mg). PET imaging performed 4 h after administration of  $^{124}\text{I}$ -anti-CEA diabody revealed rapid and specific uptake in the CEA-positive tumors (Fig. 4C), with a tumor-to-background uptake ratio of 3.99:1 (Table 1). The contrast between the CEA-positive LS174T and CEA-negative C6 xenografts was even more striking at 18 h (Figs. 4D and 4E); a ratio could not be calculated because the C6 xenografts were not distinguishable.

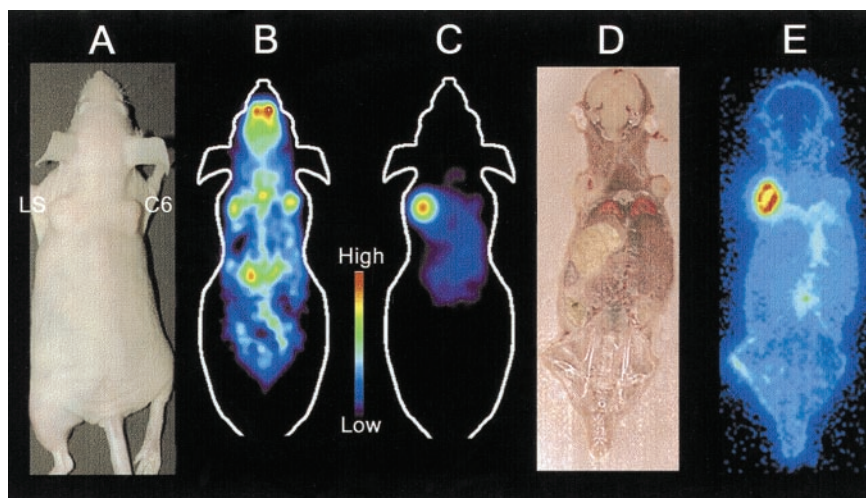


**FIGURE 3.** (A) Subcutaneous LS174T (left shoulder) and C6 glioma (right shoulder) xenografts were established in nude mouse. (B) PET imaging with  $^{18}\text{F}$ -FDG was done 2 d before injection of  $^{124}\text{I}$  (10/64 planes shown). (C) Mouse was injected with 3.1 MBq (85  $\mu\text{Ci}$ )  $^{124}\text{I}$ -minibody and imaged at 18 h by PET (10/64 planes shown). Both these images (B and C) are on same color scale. (D) After 18-h scan, mouse was euthanized and frozen, and whole-body coronal sections were cut in cryostat and processed for DWBA. (E) DWBA confirms specific localization of  $^{124}\text{I}$  minibody to CEA-positive tumor and low levels of background activity.

**TABLE 1**  
Ratios Derived from PET Data Comparing Target-to-Background Levels of <sup>124</sup>I Activity

Ratio	Minibody (n = 8)		Diabody (n = 4)	
	4 h	18 h	4 h	18 h
LS174T to C6	3.46 ± 0.72	10.85 ± 2.03*	3.99 ± 0.98	—†
LS174T to background	0.78 ± 0.10	3.48 ± 0.48*	1.83 ± 0.40	6.11 ± 1.49‡
LS174T to soft tissue	3.05 ± 0.72	11.03 ± 2.35*	3.95 ± 1.27	10.93 ± 2.21‡

\*Significantly different from 4 h (minibody group; *P* < 0.05, paired *t* test).

†Could not be calculated, as C6 tumor was not distinguishable.

‡Significantly different from 4 h (diabody group; *P* < 0.05, paired *t* test).

Data are mean ± SEM. Background is abdominal region.

### Tumor-to-Background Ratios from Serial Imaging

Imaging by PET allowed evaluation of tracer localization and distribution over time in the same animal. All animals were imaged 4 and 18 h after injection of minibody or diabody. In animals that were injected with <sup>124</sup>I-anti-CEA minibody, there was substantial activity in the blood pool at the 4-h time point and hence the tumor-to-background ratio was only about 0.8:1 (Fig. 4A; Table 1). Subsequently, this ratio improved to 3.5:1 at the 18-h time point as most of the activity in the nonspecific areas cleared, whereas the activity

in the CEA-positive tumors remained high (Fig. 4B). Background ratios of tumor to soft tissue averaged 3.05:1 at 4 h and improved to 11.03:1 at 18 h (Table 1).

Higher tumor-to-background ratios were achieved in animals administered <sup>124</sup>I-labeled anti-CEA diabody. In these animals (*n* = 4), the tumor-to-background (background in abdominal region) ratios improved from 1.8:1 at 4 h after injection (Fig. 4C) to 6.1:1 at 18 h after injection (Figs. 4D and 4E). Background ratios of tumor to soft tissue were even higher, increasing from 4:1 at 4 h to 11:1 by the 18-h scans. This improvement in the tumor-to-background ratios achieved with <sup>124</sup>I-labeled anti-CEA diabody, especially regarding the central activity in the abdominal region, provides greater contrast and renders a clear image of the CEA-positive tumor (Fig. 4E).

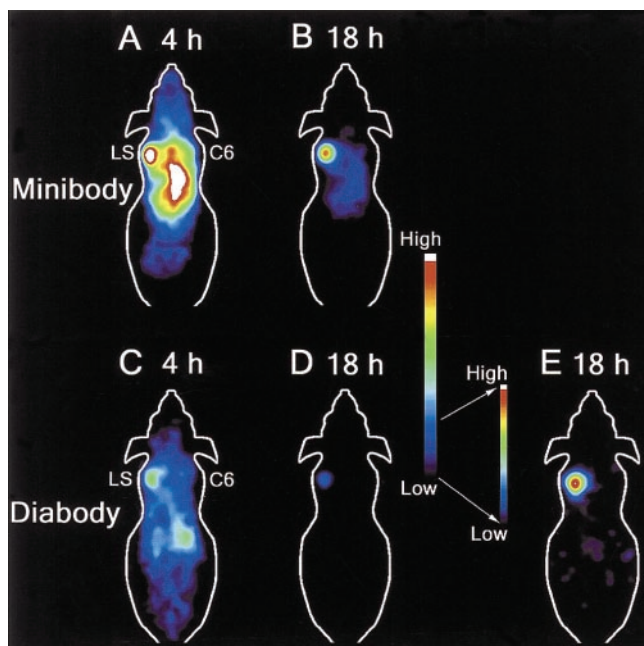


**FIGURE 4.** Comparison of <sup>124</sup>I minibody and <sup>124</sup>I diabody by serial PET imaging at 4 and 18 h. Mice bearing LS174T (LS) and C6 rat glioma (C6) xenografts were injected via tail vein with 1.9–3.1 MBq (65–85 μCi) <sup>124</sup>I minibody (A and B) or diabody (C–E) and imaged at 4 and 18 h. At 18 h, background activity in central region was minimal in <sup>124</sup>I diabody (D and E)–injected animal, resulting in high contrast, which can be seen in these *maximum a posteriori* reconstructed images (10/64 planes shown). A–D are on common scale. D was rescaled to E to illustrate excellent contrast achieved with <sup>124</sup>I diabody at 18 h.

### Tissue Counting

After the 18-h scans, animals not used in DWBA studies were sacrificed, and activity in various tissues was quantitated using a γ-counter. The results in Table 2 confirm high tumor uptake in the LS174T model, with a mean uptake of 20.55 ± 2.74 %ID/g for the <sup>124</sup>I-T84.66 minibody (*n* = 5), consistent with previous work using <sup>123</sup>I/<sup>131</sup>I-radiolabeled T84.66 minibody (5,13). Uptake of <sup>124</sup>I-minibody by the control C6 xenografts and activities in heart, liver, and kidney were significantly lower than uptake in the positive tumors, and the tumor-to-control ratios determined by counting exceeded 13:1 for the indicated tissues and were consistent with ratios determined from the PET scans.

Similarly, biodistribution data for the anti-CEA diabody (Table 2) yielded activity levels of 4.53 ± 0.50 %ID/g in the LS174T xenografts (*n* = 4) at 18 h, comparable to the previously published 4.56 ± 0.5 %ID/g at 24 h using <sup>123</sup>I-T84.66 diabody (12). Control C6 tumor activity was only 0.23 ± 0.03 %ID/g, resulting in a tumor-to-control tumor activity ratio of 21.3:1 (Table 2). The highest observed tumor-to-normal ratio was 61.6:1 for LS174T to heart. Again, these results validate the high contrast observed in the PET images using <sup>124</sup>I-diabody as the tracer.

TABLE 2

%ID/g Values and Target-to-Background (LS174T/Organ) Ratios Derived from Ex Vivo Counting of Weighed Tissues in  $\gamma$ -Counter After 18-Hour Uptake Time

Tissue	%ID/g		Ratio	
	Minibody ( <i>n</i> = 5)	Diabody ( <i>n</i> = 4)	Minibody ( <i>n</i> = 5)	Diabody ( <i>n</i> = 4)
LS174T	20.55 ± 2.74	4.53 ± 0.50*		
C6	1.87 ± 0.38†	0.23 ± 0.03*†	26.19 ± 11.16	21.31 ± 4.47
Heart	1.78 ± 0.21†	0.07 ± 0.01*†	18.93 ± 6.10	61.57 ± 7.84*
Liver	1.18 ± 0.18†	0.15 ± 0.01*†	31.05 ± 9.91	31.16 ± 3.46
Kidney	1.51 ± 0.22†	0.37 ± 0.05*†	25.73 ± 9.87	12.66 ± 2.17

\*Significantly different from minibody ( $P < 0.05$ , unpaired *t* test).

†Significantly different from LS174T (minibody group;  $P < 0.05$ , paired *t* test).

‡Significantly different from LS174T (diabody group;  $P < 0.05$ , paired *t* test).

Data are mean ± SEM.

## DISCUSSION

The present intermediate-molecular-weight engineered anti-CEA antibody fragments, T84.66 minibody and diabody, demonstrated excellent targeting and imaging properties when labeled with  $^{124}\text{I}$  and evaluated in an athymic mouse/tumor xenograft model by PET. Confirming previous work, mean tumor uptake levels of 20.55 %ID/g (minibody) or 4.5 %ID/g (diabody) were achieved at 18 h after administration. Fast blood clearance, combined with metabolism and clearance of radioiodine activity from peripheral tissues, leads to high ratios of tumor to normal activity and excellent visualization using either fragment by 18 h. Tumors as small as 11 mg were detected by small-animal PET. High ratios of tumor (LS174T) to control tumor (C6) localization were achieved, demonstrating specificity, although this conclusion may be somewhat tempered by the use of a different tumor type as control. It will be important to confirm these results in paired xenografts that differ only in CEA expression.

Development of tracers for radioimmunoimaging requires attention to at least 3 main components: target antigen, antibody (including format), and radionuclide. Carcinoembryonic antigen, a classic tumor-associated antigen in colorectal carcinoma as well as other adenocarcinomas, remains a prime target for antibody-based detection and therapeutic applications (23). The anti-CEA minibody and diabody were derived from T84.66, a high-affinity ( $K_A = 2 \times 10^{11}$  L/mol), highly specific antibody that recognizes an epitope on the A3 domain of CEA (24). Previous studies demonstrated the favorable tumor-targeting properties of these fragments labeled with radioiodine or  $^{111}\text{In}$  in LS174T-xenografted mice (5,12,13). However, radiometal-labeled fragments showed retention of activity in liver (minibody) or kidney (diabody). The T84.66 minibody was radiolabeled with  $^{64}\text{Cu}$ , a positron-emitting radiometal with a 12.7-h half-life, to explore its utility as a PET tracer (15). Excellent tumor localization was observed, but as expected, liver activity was elevated, limiting imaging applications to extrahepatic sites.

The present work demonstrated that radiolabeling of the anti-CEA minibody and diabody using  $^{124}\text{I}$  for PET imaging preserves the excellent tumor targeting of these fragments while enhancing the overall images because of lower background activity in normal tissues. The question arises as to which of these fragments is preferable as an imaging agent. The T84.66 minibody reaches higher absolute activity levels in tumor, but background activity takes longer to clear and is still apparent at 18 h in the murine model. By contrast, radioactivity delivered to the CEA-positive xenografts by diabody is substantially lower; however, this apparent disadvantage is ameliorated by the much lower background activity seen in the mouse. Further optimization of diabody radioiodination to retain high immunoreactivity should also enhance performance. In this animal imaging model, the diabody appears to have the advantage over the minibody in achieving higher overall contrast; however, performance still needs to be evaluated in the clinic.

Guidance on the selection of an appropriate fragment can be provided by analysis such as calculation of the imaging figure of merit (IFOM) (25), an approach based on determining statistically the required counting time to distinguish tumor from blood background. We calculated IFOM values for  $^{124}\text{I}$ -labeled fragments from previously published biodistribution data on radioiodinated minibody and diabody. Results (not shown) suggested that the minibody should be the superior agent, with an optimal imaging time of 20–24 h after administration, and the optimal imaging interval for the diabody would be 8–12 h. However, the current IFOM calculations are dependent on tumor size and do not take into account normal tissue activity. Further PET imaging studies at additional time points will clarify some of these issues, as will human tumor targeting and pharmacokinetic data from ongoing clinical imaging studies of  $^{123}\text{I}$ -T84.66 minibody. Either of these fragments labeled with  $^{124}\text{I}$  may prove especially useful for imaging hepatic metastases.

Several groups have explored the use of  $^{124}\text{I}$  for PET imaging with clinical scanners, including antibody applications. Bakir et al. (8) demonstrated detection of c-erbB2/

Her2-overexpressing tumor xenografts in athymic mouse using  $^{124}\text{I}$ -ICR12, a rat monoclonal antibody. Tumors as small as 6 mm in diameter were imaged at 24, 48, and 120 h. More recently, Lee and associates (7) imaged human colon carcinoma xenografts using humanized  $^{124}\text{I}$ -A33 monoclonal antibody. This intact antibody reached 50 %ID/g 4 d after injection, and clear tumor images (tumor sizes, 0.2–0.7 g) were obtained when mice were imaged at 24, 48, or 240 h after injection. Clinical investigations have included PET imaging of breast cancer patients using  $^{124}\text{I}$ -anti-mucin antibodies (10) and evaluation of  $^{124}\text{I}$ -3F9 antibody administration for dose estimation in a patient with neuroblastoma (26). Use of a positron-emitting radionuclide with a long physical half-life, such as  $^{124}\text{I}$ , has been necessary for applications using intact antibodies because of their extended biologic half-lives. As noted in the above literature, optimal imaging was obtained days after administration. Results presented here indicate that  $^{124}\text{I}$  is also well suited for imaging using engineered fragments, with the added advantage of shorter intervals to optimal imaging times (same day or next day).

The use of  $^{124}\text{I}$  for radiolabeling the anti-CEA fragments, in particular the minibody, provides advantages over previous work. As expected, the high, persistent liver activity observed in our previous PET studies using  $^{64}\text{Cu}$ -anti-CEA minibody was dramatically reduced because of the different metabolism and clearance of activity after administration of radioiodinated protein compared with radiometal-labeled protein. The fact that CEA is not internalized on binding of antibody probably contributes to retention of activity in the LS174T xenografts, enhancing the tumor-to-liver and tumor-to-kidney ratios of the  $^{124}\text{I}$ -diabodies and -minibodies. In addition to the favorable biologic properties of these radioiodinated proteins,  $^{124}\text{I}$ -minibody and -diabody should also offer the advantage of high avidity compared with  $^{99\text{m}}\text{Tc}$ -labeled Fab' fragment (arcitumomab [CEA-Scan]; Immunomedics, Inc.), as these represent high-affinity bivalent, rather than monovalent, CEA-binding proteins.

The present work suggests that qualitative PET imaging using  $^{124}\text{I}$ -engineered fragments may provide a sensitive method for visualization of tumor masses. Relative quantitation (determination of target-to-background ratios) is straightforward. However, absolute quantitation of  $^{124}\text{I}$  activity will require correction of the imaging data to compensate for the unfavorable spectrum of emissions generated during the decay of  $^{124}\text{I}$ . In particular,  $^{124}\text{I}$  decay results in only a 23% yield of positrons, compared with the near 100% positron yield of  $^{18}\text{F}$  (27). The average energy of the  $^{124}\text{I}$  positrons is higher than that for  $^{18}\text{F}$ , and the increased positron range would result in degradation of resolution.  $^{124}\text{I}$  also has a complex decay scheme, resulting in a high  $\gamma$ -component, with many high-energy  $\gamma$ -emissions occurring in coincidence with each other and with the annihilation photons. Despite these shortcomings, PET imaging studies using phantoms or xenografted mouse models have

been conducted under realistic conditions. Results indicate that suitable images could be obtained and that relative quantitation was feasible using a variety of clinical PET scanners (11,27). Recently, a Monte Carlo simulation scheme has been developed for correction of  $^{124}\text{I}$  images for scatter,  $\gamma$ -coincidences, and attenuation and should be applicable to the small-animal PET data generated in the current studies (C. Holdsworth, oral communication, May 2003). Correction of the current datasets is in progress. A final challenge in the current work arises from the small size of some of the tumors used—close to the resolution of the prototype small-animal PET instrument (1.8–2.0 mm). As a result, correction for the partial-volume effect will also be required for accurate quantitation (28).

The present approach can be highly complementary to existing PET oncology imaging, which primarily uses  $^{18}\text{F}$ -FDG as a tracer for glucose uptake and use by cancer cells. Direct comparison of quantitative image analysis was not attempted here because of the complexity of the  $^{124}\text{I}$  emissions as noted above. However, it is apparent from Figure 3 (which presents raw images of the same tumor-bearing mouse imaged using both tracers on the same color scale) that antibody-fragment imaging resulted in highly specific tumor localization in this xenograft model, when compared with  $^{18}\text{F}$ -FDG. Uptake levels for the engineered fragments equal (diabody) or substantially exceed (minibody) the %ID/g levels attained by  $^{18}\text{F}$ -FDG (which maximizes at approximately 3–8 %ID/g depending on the tumor model). Imaging modes such as antibody-based imaging would be especially useful as an alternative to  $^{18}\text{F}$ -FDG PET in cancers that exhibit low metabolic activity such as low-grade lymphomas, many prostate cancers, and other indolent tumors. There are many well-characterized tumor-associated antigens currently under evaluation for antibody-targeted imaging and therapy in lymphomas and solid tumors, such as CD20, Her2, and TAG-72, that could similarly be targeted using  $^{124}\text{I}$ -radiolabeled recombinant fragments.

## CONCLUSION

The combination of  $^{124}\text{I}$  and an appropriate genetically engineered antibody fragment can provide a new class of PET tracers for imaging tumors on the basis of cell-surface antigen expression. Evaluation of  $^{123}\text{I}$ -T84.66 minibody for  $\gamma$ -camera/SPECT imaging in patients is in progress. Results from these studies and  $^{123}\text{I}$ -diabody studies will guide selection of appropriate  $^{124}\text{I}$ -labeled recombinant fragment for clinical PET studies. Furthermore, current progress in the genomics and proteomics of cancer is rapidly generating new molecular targets that can potentially be accessed using antibody technology. Reformatting of antibodies into diabodies or minibodies for  $^{124}\text{I}$  radiolabeling can provide a rapid route for generation of new PET tracers for cancer imaging.

## ACKNOWLEDGMENTS

We are thankful to Dr. David Stout, Judy Edwards, and Waldemar Ladno for providing expert technical help with PET imaging, and to Khoi Nguyen and Xiaoman Zhou Lewis for their help with animal studies. We are also grateful to Dr. Clay Holdsworth and Andreas Loening for their valuable suggestions on image reconstruction and analysis. Appreciations are due to Chia-Wei Cheung and to Anne-Line Anderson for conducting the protein purification and radioiodination. This study was supported by the National Institutes of Health/National Cancer Institute (SAIRP-R24-CA-92845, NCI-CA-43904, NCI-CA-33572, NCI-CA-08748, and NCI-CA-86438), the Department of Defense (DAMD-17-00-1-0150), and the Department of Energy (DE-F02-86-E60407 and DE-FC03-87ER60615).

## REFERENCES

1. Colcher D, Goel A, Pavlinkova G, Beresford G, Booth B, Batra SK. Effects of genetic engineering on the pharmacokinetics of antibodies. *Q J Nucl Med.* 1999;43:132–139.
2. Wu AM, Yazaki PJ. Designer genes: recombinant antibody fragments for biological imaging. *Q J Nucl Med.* 2000;44:268–283.
3. Huston JS, George AJ, Adams GP, et al. Single-chain Fv radioimmunotargeting. *Q J Nucl Med.* 1996;40:320–333.
4. Yokota T, Milenic DE, Whitlow M, Wood JF, Hubert SL, Schlom J. Microautoradiographic analysis of the normal organ distribution of radioiodinated single-chain Fv and other immunoglobulin forms. *Cancer Res.* 1993;53:3776–3783.
5. Hu S, Shively L, Raubitschek A, et al. Minibody: a novel engineered anti-carcinoembryonic antigen antibody fragment (single-chain Fv-CH3) which exhibits rapid, high-level targeting of xenografts. *Cancer Res.* 1996;56:3055–3061.
6. Slavin-Chiorini DC, Kashmiri SV, Schlom J, et al. Biological properties of chimeric domain-deleted anticarcinoma immunoglobulins. *Cancer Res.* 1995;55:5957s–5967s.
7. Lee FT, Hall C, Rigopoulos A, et al. Immuno-PET of human colon xenograft-bearing BALB/c nude mice using <sup>124</sup>I-CDR-grafted humanized A33 monoclonal antibody. *J Nucl Med.* 2001;42:764–769.
8. Bakir MA, Eccles S, Babich JW, et al. c-erbB2 protein overexpression in breast cancer as a target for PET using iodine-124-labeled monoclonal antibodies. *J Nucl Med.* 1992;33:2154–2160.
9. Rubin SC, Kairemo KJ, Brownell AL, et al. High-resolution positron emission tomography of human ovarian cancer in nude rats using <sup>124</sup>I-labeled monoclonal antibodies. *Gynecol Oncol.* 1993;48:61–67.
10. Wilson CB, Snook DE, Dhokia B, et al. Quantitative measurement of monoclonal antibody distribution and blood flow using positron emission tomography and <sup>124</sup>I-iodine in patients with breast cancer. *Int J Cancer.* 1991;47:344–347.
11. Pentlow KS, Graham MC, Lambrecht RM, et al. Quantitative imaging of iodine-124 with PET. *J Nucl Med.* 1996;37:1557–1562.
12. Wu AM, Williams LE, Zieran L, et al. Anti-carcinoembryonic antigen (CEA) diabody for rapid tumor targeting and imaging. *Tumor Targeting.* 1999;4:47–58.
13. Yazaki PJ, Wu AM, Tsai SW, et al. Tumor targeting of radiometal labeled anti-CEA recombinant T84.66 diabody and T84.66 minibody: comparison to radioiodinated fragments. *Bioconjug Chem.* 2001;12:220–228.
14. Arano Y. Strategies to reduce renal radioactivity levels of antibody fragments. *Q J Nucl Med.* 1998;42:262–270.
15. Wu AM, Yazaki PJ, Tsai S, et al. High-resolution microPET imaging of carcinoembryonic antigen-positive xenografts by using a copper-64-labeled engineered antibody fragment. *Proc Natl Acad Sci USA.* 2000;97:8495–8500.
16. Yazaki PJ, Shively L, Clark C, et al. Mammalian expression and hollow fiber bioreactor production of recombinant anti-CEA diabody and minibody for clinical applications. *J Immunol Methods.* 2001;253:195–208.
17. Bebbington CR, Renner G, Thomson S, King D, Abrams D, Yarranton GT. High-level expression of a recombinant antibody from myeloma cells using a glutamine synthetase gene as an amplifiable selectable marker. *Biotechnology.* 1992;10:169–175.
18. You YH, Hefta LJ, Yazaki PJ, Wu AM, Shively JE. Expression, purification, and characterization of a two domain carcinoembryonic antigen minigene (N-A3) in *Pichia pastoris*: the essential role of the N-domain. *Anticancer Res.* 1998;18:3193–3201.
19. Sheh Y, Kozirowski J, Balatoni J, Lom C, Dahl JR, Finn RD. Low energy cyclotron production and chemical separation of “no carrier added” iodine-124 from a reusable, enriched tellurium-124 dioxide/aluminum oxide solid solution target. *Radiochim Acta.* 2000;88:169–173.
20. Chatziioannou AF, Cherry SR, Shao Y, et al. Performance evaluation of microPET: a high-resolution lutetium-124 oxyorthosilicate PET scanner for animal imaging. *J Nucl Med.* 1999;40:1164–1175.
21. Kinahan PE, Rogers JG. Analytic 3D image reconstruction using all detected events. *IEEE Trans Nucl Sci.* 1989;36:964–968.
22. Qi J, Leahy RM, Cherry SR, Chatziioannou A, Farquhar TH. High-resolution 3D Bayesian image reconstruction using the microPET small-animal scanner. *Phys Med Biol.* 1998;43:1001–1013.
23. Goldenberg DM. Carcinoembryonic antigen as a target cancer antigen for radio-labeled antibodies: prospects for cancer imaging and therapy. *Tumour Biol.* 1995;16:62–73.
24. Neumaier M, Shively L, Chen FS, et al. Cloning of the genes for T84.66, an antibody that has a high specificity and affinity for carcinoembryonic antigen, and expression of chimeric human/mouse T84.66 genes in myeloma and Chinese hamster ovary cells. *Cancer Res.* 1990;50:2128–2134.
25. Williams LE, Liu A, Wu AM, et al. Figures of merit (FOMs) for imaging and therapy using monoclonal antibodies. *Med Phys.* 1995;22:2025–2027.
26. Larson SM, Pentlow KS, Volkow ND, et al. PET scanning of iodine-124-3F9 as an approach to tumor dosimetry during treatment planning for radioimmunotherapy in a child with neuroblastoma. *J Nucl Med.* 1992;33:2020–2023.
27. Pentlow KS, Graham MC, Lambrecht RM, Cheung NK, Larson SM. Quantitative imaging of I-124 using positron emission tomography with applications to radioimmunodiagnosis and radioimmunotherapy. *Med Phys.* 1991;18:357–366.
28. Hoffman EJ, Huang SC, Phelps ME. Quantitation in positron emission computed tomography: 1. Effect of object size. *J Comput Assist Tomogr.* 1979;3:299–308.